# PCCP



## **PAPER**



Cite this: Phys. Chem. Chem. Phys., 2022. 24. 23884

# Desorption trends of small alcohols and the disruption of intermolecular interactions at defect sites on Au(111)†

Eric M. Maxwell, a Lyssa A. Garber, a Clayton J. Rogers, Ava J. Galgano, a Jordon S. Baker, ab Hasan Kaleem, David T. Boyle, ac Jessica L. Berry and Ashleigh E. Baber \*\*

Gold-based catalysts have received tremendous attention as supports and nanoparticles for heterogeneous catalysis, in part due to the ability of nanoscale Au to catalyze reactions at low temperatures in oxidative environments. Surface defects are known active sites for low temperature Au chemistry, so a full understanding of the interplay between intermolecular interactions and surface morphology is essential to an advanced understanding of catalytic behavior and efficiency. In a systematic study to better understand the adsorption and intermolecular behavior of small alcohols ( $C_1$ - $C_4$ ) on Au(111) defect sites, coverage studies of methanol, ethanol, 1-propanol, 1-butanol, 2-butanol, and isobutanol have been conducted on Au(111) using ultrahigh vacuum temperature programmed desorption (UHV-TPD). These small alcohols molecularly adsorb on the Au(111) surface and high resolution experiments reveal distinct terrace, step edge, and kink adsorption features for each molecule. The hydrogenbonded (H-bonded) networks of small alcohols on Au(111), except for 1-butanol and isobutanol, have been previously imaged on the molecular level at low temperatures by scanning tunneling microscopy. Primary C<sub>1</sub>-C<sub>3</sub> alcohols exhibit planar H-bonded long extended zigzag chain networks while 2-butanol arranges in tetramer clusters of H-bonded molecules due to steric hindrance inhibiting the proximity of molecules on Au(111). Herein, the desorption energy of small primary alcohols was shown to trend linearly with increasing  $C_1$ - $C_4$  carbon chain length, indicating that the H-bonded molecular packing of 1-butanol resembles that of methanol, ethanol, and 1-propanol, while isobutanol and 2-butanol deviate from the trend. Butanol isomer studies allow the prediction of isobutanol long extended chains in contrast to tetramers. The distinction between the desorption of butanol isomers highlights the role of intermolecular interactions due to the difference in molecular packing structures on Au(111). Furthermore, by studying the energetics of terrace H-bonded networks in comparison with molecular adsorption at undercoordinated step edge and kink defect sites, it is shown that the contribution of stabilizing van der Waals forces to the overall adsorption energy is less for small alcohols adsorbed at kink sites (3.1 kJ mol<sup>-1</sup> per CH<sub>2</sub>) and similar for those adsorbed at step edge (4.8 kJ mol<sup>-1</sup> per CH<sub>2</sub>) and Au terrace sites (4.9 kJ  $\text{mol}^{-1}$  per CH<sub>2</sub>).

Received 2nd December 2021, Accepted 20th September 2022

DOI: 10.1039/d1cp05509g

rsc.li/pccp

### Introduction

The partial oxidation of alcohols has received great interest in recent years, as the industrially relevant products of these

reactions are often produced in inefficient or ecologically harmful methods that may be solved by the promising results of catalytic studies. 1-9 Metallic nanoparticle defects have been identified as active sites for these reactions in multiple studies<sup>8,10–12</sup> and so, the characterization of the fundamental interactions between alcohols and these sites, including metallic terraces, step edges, and kink sites, must be completed experimentally. Additionally, fundamental studies have been conducted to determine the role of weaker forces for selectivity and overall reaction efficiency. In one such study, the role of van der Waals (vdW) interactions between the carbon chains of reactive intermediates and Au(111) significantly affected

<sup>&</sup>lt;sup>a</sup> Department of Chemistry and Biochemistry, James Madison University, Harrisonburg, VA 22807, USA. E-mail: baberae@jmu.edu

<sup>&</sup>lt;sup>b</sup> Department of Chemistry, Virginia Commonwealth University, Richmond, VA 23284. USA

<sup>&</sup>lt;sup>c</sup> Department of Chemistry, Stanford University, Stanford, CA 94305, USA

<sup>†</sup> Electronic supplementary information (ESI) available: High coverage temperature programmed desorption plots and tabulated desorption energies of all alcohols studied. See DOI: https://doi.org/10.1039/d1cp05509g

relative stability and selectivity. 13 In the interest of better understanding the role of weak forces in heterogeneouslycatalysed reactions on surfaces, this study identifies and explores the role of vdW adsorbate/surface interactions as well as intermolecular H-bonding interactions on adsorption energies of small alcohols on Au(111) and how surface morphology affects these interactions. These model studies provide a benchmark for alcohol H-bonded networks, that could be extended to water, which is ubiquitous and is a known promotor in oxidation reactions over metal/oxide catalysts. 14-20

On Au(111), primary alcohols methanol (MeOH), ethanol (EtOH), and 1-propanol (1-PrOH) form long extended H-bonded chains, while the secondary alcohol, 2-butanol (2-BuOH), forms tetramer units containing four H-bonded molecules each. 10,21-24 Liquid atomic force microscopy (AFM) images of alcohol/water mixtures for MeOH, EtOH, and 1-PrOH exhibit long extended chains as well.<sup>25,26</sup> The molecular packing structures for primary alcohols 1-butanol (1-BuOH) and isobutanol (i-BuOH) have yet to be imaged on Au(111) using low temperature scanning tunnelling microscopy (STM). Previous temperature programmed desorption (TPD) studies for MeOH, EtOH, 1-PrOH and 2-BuOH on Au(111) have focused on the desorption from terraces and multilayers as control studies for their reaction on atomic oxygen on Au(111), however intermolecular interactions were not systematically studied. 1,3-5 None of the alcohol intermolecular networks have been investigated at undercoordinated defect sites (step edges, kink sites), but EtOH bonded at undercoordinated Au(111) edge dislocations at herringbone elbows have been previously shown to form sub-optimal surface structures (pentamers) that do not match with theoretically maximized intermolecular interactions (extended H-bonded chains).<sup>24</sup> These structures are representative of the interplay between surface features and intermolecular interactions between adsorbate molecules.

Previous density functional theory (DFT) calculations of 2-BuOH on Au(111) tracked surface-adsorbate and adsorbateadsorbate forces with increasing molecule cluster size. A 2-BuOH monomer showed the strongest surface-adsorbate bond, in contrast to tetramers and hexamers, which displayed greater overall binding energy due to adsorbate-adsorbate interactions even though the surface-adsorbate bond was actually weaker.<sup>27</sup> This stabilization through intermolecular lateral interactions can be extrapolated to kink site adsorption where the molecules are isolated from neighbouring molecules due to the local atomic surface structure.

The assignment of ethanol adsorption to defect sites on Au(111) and Ag(111) has been previously reported.<sup>6,28</sup> TPD experiments were conducted for each sample following Ar+ ion sputtering to induce defects to aid in the identification of undercoordinated adsorption sites.<sup>6,28</sup> DFT calculations showed trends in the adsorption energies for ethanol adsorbed to step edge and kink sites supporting the TPD desorption features.<sup>28</sup> Previous results on MeOH/Au(111) assigned higher temperature desorption features to repulsive molecular interactions on terrace sites,5 yet due to the combination of TPD sputtering experiments with DFT calculations, the higher temperature desorption features are interpreted as step edge and

kink site defects in this paper. The identification of CO adsorption on Au(111) step edges and kink sites after Ar<sup>+</sup> sputtering has also been described using TPD, STM, and DFT. CO was found to desorb at 130 K and 170 K, which were related to CO adsorption at steps and kinks with a coordination number of 6, respectively, on Au(111).<sup>29</sup>

Herein, TPD was used to study the intermolecular interactions between primary alcohols MeOH, EtOH, 1-PrOH, 1-BuOH, 2-BuOH, and i-BuOH on Au(111) terraces, as well as the desorption energetics of the disruptions of those intermolecular interactions at step edge and kink defect sites. TPD can quantitatively compare weak intermolecular interactions such as dispersion forces to better correlate theory and experiment.<sup>30</sup> The results shown here feature TPD of pure 1-BuOH and i-BuOH which have not vet been studied by TPD or STM on Au(111). Analysis of the desorption trends for small alcohols allows the prediction of unknown thermodynamically stabilized molecular packing structures on Au(111), namely those for 1- and i-BuOH. Additionally, the subtle differences between desorption energies of alcohols on terraces and defect sites have been measured and compared. These experimental energetic differences can be used to understand the relationship of coordination number and intermolecular interactions for catalytically relevant molecular precursors on defect sites, in particular, those that are known active sites on metallic nanoparticles. Overall, this study provides key insight into how intermolecular interactions can tune the interaction of molecular substrates with heterogeneous catalysts, which can guide future catalyst design.

# Experimental

Experiments were performed in an ultrahigh vacuum (UHV) TPD chamber. The UHV chamber is pumped by a turbomolecular pump and operates at a base pressure of  $\sim 5 \times 10^{-10}$  Torr during experiments. The chamber contains a quadrupole mass spectrometer (Hiden HAL 3F 301 RC) for TPD and residual gas analysis. The average linear heating rate  $(\beta)$  for TPD experiments was 1.07  $\pm$  0.21 K s<sup>-1</sup> and is reported in each figure caption. Collimated high-precision leak valves were used for controlling gas doses into the chamber. A Au(111) single crystal (Princeton Scientific) was mounted on a sample holder and held vertically by tungsten wires (Goodfellow, 99.95%, 0.25 mm diameter) between two copper blocks in the centre of the chamber, which allowed the sample to be resistively heated and cooled with liquid nitrogen. Temperature measurements were recorded with a k-type thermocouple that was directly attached to a hole in the side of the Au(111) crystal. The Au(111) surface was prepared via cycles of 0.5 keV Ar<sup>+</sup> sputtering and annealing in UHV at  $\sim 875-950$  K. The sample was cleaned between each species' TPD coverage study. Sigma-Aldrich HPLC grade ≥99.9% methanol, PHARMCO-AAPER 200 proof-absolute anhydrous ACS/USP grade ethanol, Sigma-Aldrich HPLC grade ≥99.9% 1-propanol, Sigma-Aldrich 99.9% 1-butanol, Sigma-Aldrich anhydrous 99.5% 2-butanol, and Sigma-Aldrich anhydrous

99.5% 2-methyl-1-propanol (isobutanol) were all purified by successive freeze/pump/thaw cycles. A desiccant (ACROS Organics Molecular sieves 5A, 8 to 12 mesh) was heated to drive off water, cooled, and then added to the 1-BuOH, 2-BuOH, and i-BuOH dosing glass ampules prior to freeze/pump/thaw cycles. All butanol sample lines needed to be gently annealed to facilitate consistent dosing. The saturation coverage of each alcohol is defined as 1 monolayer (ML) and was calculated using TPD experiments. Coverages are reported in relative monolayers as determined by total area under the curve for traces with saturated surface desorption features (terrace, step edge, and kink site). Mass to charge (m/z) ratios for each alcohol were chosen based on the fragment with the greatest intensity: methanol m/z = 31, ethanol m/z = 31, 1-propanol m/z = 31, 1-butanol m/z = 31, 2-butanol m/z = 45, isobutanol m/z = 43. While the m/z = 56 fragment for 1-butanol is slightly greater than that of m/z = 31, the two TPD plots traced each other, and the m/z = 31 is shown herein. It is well established that small alcohols do not dissociate on  $Au(111)^{1,3-6,31-33}$  and the m/zratios studied herein do not indicate dissociation, as shown in the ESI† in Fig. S7-S12.

### Results and discussion

#### Primary alcohol desorption

High resolution sub-monolayer TPD studies of MeOH, EtOH, 1-PrOH, 1-BuOH, 2-BuOH, and i-BuOH on Au(111) reveal distinct terrace, step edge, and kink adsorption sites. MeOH, EtOH, and 1-PrOH high resolution TPD spectra are shown in Fig. 1. At near monolayer coverages, the terrace desorption feature dominates, but small, high-temperature desorption features have previously been identified and characterized as desorption of molecules adsorbed to step edge (coordination number (CN) = 7-8) and kink sites (CN = 5-6), as compared to terrace (CN = 9) for EtOH on Au(111)<sup>6</sup> and Ag(111).<sup>28</sup> Fig. 2 highlights distinct adsorption sites corresponding to undercoordinated step edge (CN = 7 shown in the red circle) and kink (CN = 6 shown by the blue square) sites. Repeat experiments showed the desorption character of all molecules studied to be reproducible. Thus, in good agreement with previous works for MeOH, EtOH, 1-PrOH, and 2-BuOH, 1,3-6 we conclude that all small alcohols studied herein desorb molecularly from the Au(111) surface and exhibit first order desorption for monolayer adsorption sites. The desorption of pure 1-BuOH and i-BuOH from Au(111) has yet to be shown in the literature but exhibited expected desorption features based on other small alcohols. Full TPD coverage studies for each species were performed up to multilayer coverages, which are provided in the ESI.† Surface site desorption temperatures for all molecules studied are compiled in Table 1.

Fig. 1 shows the sub-monolayer desorption features for MeOH, EtOH, and 1-PrOH on Au(111). As shown in Fig. 2(A), MeOH (m/z = 31) desorption from Au(111) occurred at the lowest temperatures of all molecules studied. A high temperature feature at 202 K populates first at low coverages ( $\sim 0.02$  ML) and is

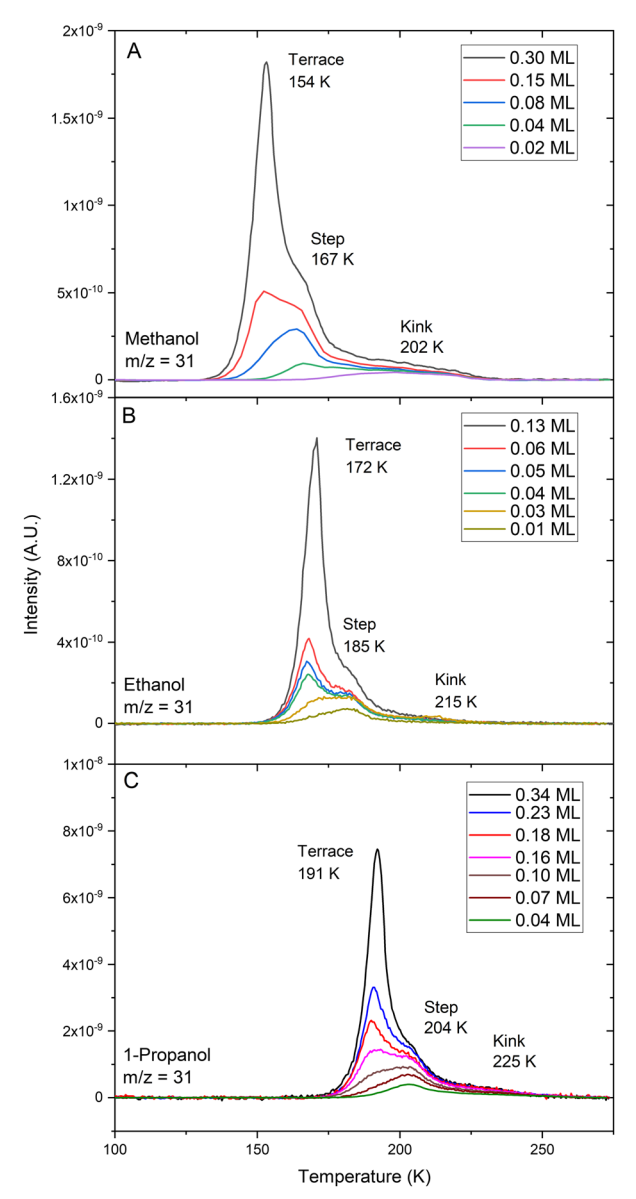


Fig. 1 Sub-monolayer coverage desorption of (A) MeOH  $(m/z=31, \beta=1.19\pm0.03~{\rm K~s^{-1}})$ , (B) EtOH  $(m/z=31, \beta=1.05\pm0.07~{\rm K~s^{-1}})$  and (C) 1-PrOH  $(m/z=31, \beta=0.95\pm0.10~{\rm K~s^{-1}})$  from Au(111). The peaks observed relate to the desorption of alcohols adsorbed to terrace, step edge, and kink sites, as labelled in the spectra.

assigned to MeOH adsorbed to kink sites. At a coverage of 0.04 ML, step edge defect sites begin to populate, and a corresponding desorption feature at 167 K grows. The terrace desorption feature (154 K) dominates at coverages greater than 0.15 ML. At coverages beyond 1 ML, a low temperature desorption feature forms at 139 K and is assigned to multilayer desorption (shown in Fig. S1, ESI†). Terrace and multilayer desorption temperatures are in good agreement with previous studies of MeOH on clean Au.<sup>5</sup>

The desorption of EtOH (m/z = 31) adsorbed to Au(111) defects<sup>6</sup> and terraces<sup>3,6</sup> has been previously reported (in the ESI†)<sup>3</sup> and is shown in Fig. 1(B) and Fig. S2 (ESI†). The desorption feature at 185 K populates first at low coverages

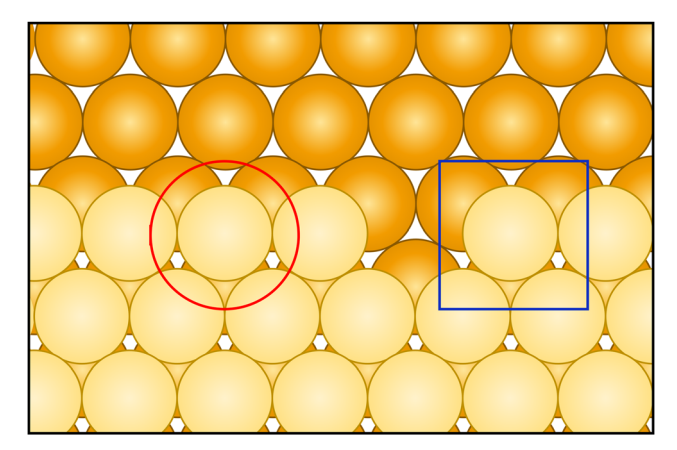


Fig. 2 Model for defect sites: step edge (red circle, CN = 7) and kink sites (blue square, CN = 6).

Table 1 Desorption temperatures (K) of all molecules and sites studied. Multilaver (multi) and terrace (monolaver) desorption features for MeOH. EtOH, 1-PrOH, and 2-BuOH are in good agreement with previous literature<sup>1,3-5</sup>

	Desorption temperatures (K)					
	МеОН	EtOH	1-PrOH	1-BuOH	2-BuOH	i-BuOH
Multi-	139	145, 150	159, 176	189	175	157, 170
Terrace	154	172	191	210	194	199
Step	167	185	204	222	211	211
Kink	202	215	225	236	227	226

and is assigned to desorption of EtOH bound to step edges. Desorption of EtOH from terrace sites dominates at coverages above 0.03 ML and occurs at 172 K, and a desorption feature at 215 K represents kink sites. While kink site adsorption is preferential, the low concentration of these sites on the Au surface during these experiments results in a desorption feature that is not significantly populated until higher coverages for most of the small alcohols.

The desorption behaviour of 1-PrOH (m/z = 31) is shown in Fig. 1(C). The step edge desorption feature at 204 K populates at the lowest coverages studied. Desorption from terrace sites occurs at 191 K, and this feature dominates above coverages of 0.18 ML. A small, high energy desorption feature is seen at 225 K, corresponding to kink sites. Terrace site desorption temperatures are in good agreement with other work on the desorption of 1-PrOH from Au(111),4 though the only multilayer desorption feature reported by Gong et al. occurs at ~160 K. Herein, the first multilayer desorption feature occurs at 176 K. The second multilayer desorption feature at 159 K appears beyond 4.32 ML, as shown in Fig. S3 (ESI†). Of methanol, ethanol, and 1-propanol, methanol is the only small alcohol that preferentially binds to the kink sites at the temperatures studied. As there are presumed similar defect concentrations each time, through identical cleaning cycles, the difference in adsorption for methanol is likely related to differences in molecular diffusion at low temperatures on Au(111).

#### **Butanol** isomer desorption

The desorption behaviour of 1-BuOH from the Au(111) surface was previously uncharacterized, and a study of this system reveals similar features to that of other small alcohols, as shown in Fig. 3 and Fig. S4 (ESI†). While the higher coverage studies (Fig. S4, ESI†) are helpful in the initial identification of defect sites, lower coverages are useful to obtain defect site adsorption features from TPD plots. High temperature features at 236 K and 223 K appear at 0.18 ML corresponding to 1-BuOH adsorbed at kink sites and step edges respectively. As shown in Fig. 3, kink site features are not observed at the lowest coverages studied (0.06 ML), likely due to the low concentration of these defect sites on the surface combined with the low mobility of larger molecules on Au(111) at the temperatures studied. Interestingly, a much more substantial high temperature tail is observed for 1-BuOH, than the other small alcohols studied. This is potentially related to the increased intermolecular interactions between 1-BuOH molecules, as will be discussed later, but studies of higher order alcohols would need to be conducted to test that hypothesis. The terrace site desorption feature at 210 K begins to dominate at 0.34 ML. A low temperature desorption feature at 187 K appears at higher coverages and corresponds to multilayer desorption, shown in Fig. S4 (ESI†).

The desorption of 2-BuOH from the Au(111) surface is shown in Fig. 4. The most intense mass fragment, m/z = 45 is shown and traces with m/z = 59, which is the parent fragment. The desorption temperature for the terrace peak is in good agreement with previous studies. The heating rate for these experiments was 1.5 K s<sup>-1</sup>; while this differs from other studies, the slight increase in heating rate is not significant enough to undermine a comparison of desorption temperatures or more importantly, desorption energies calculated from the Redhead first order approximation. The desorption of 2-BuOH bound to step edge defect sites is seen at the lowest coverages and occurs

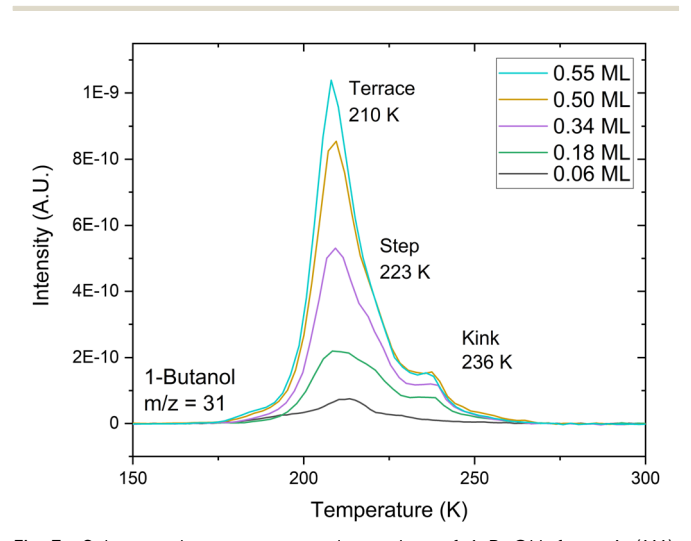


Fig. 3 Sub-monolayer coverage desorption of 1-BuOH from Au(111), m/z = 31 is reported and traces with m/z = 56 for all experiments  $(\beta = 1.15 \pm 0.05 \text{ K s}^{-1}).$ 

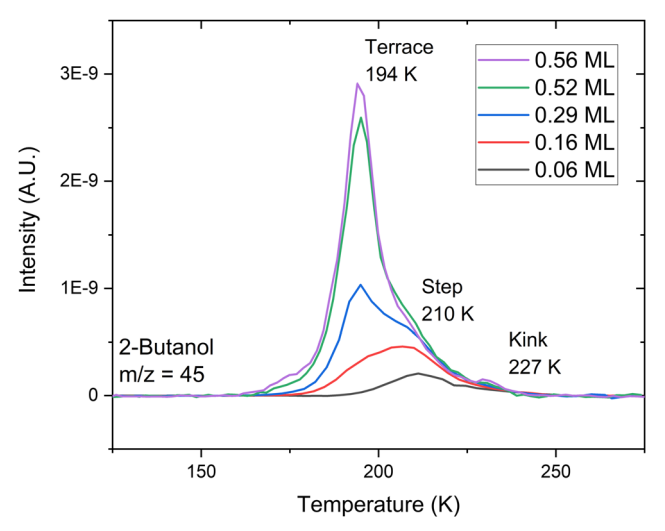


Fig. 4 Sub-monolayer desorption of 2-BuOH from Au(111), m/z = 45reported and traces with m/z = 59 for all experiments, ( $\beta = 1.52 \pm 0.05$  K s<sup>-1</sup>).

at 210 K. With increasing coverage, the terrace site desorption feature appears at 194 K and dominates at coverages greater than 0.29 ML. A small kink site desorption feature grows with increasing coverage at 227 K. Multilayer desorption occurs at 175 K and is seen at higher coverages, shown in Fig. S5 (ESI†). The desorption peaks for 2-BuOH (Fig. 4) occur at significantly lower temperatures than 1-BuOH (Fig. 3) for all sites.

The desorption behaviour of i-BuOH from the Au(111) surface is shown in Fig. 5. The most intense mass fragment, m/z = 43, is shown and traces with m/z = 31. Step edge desorption features at 211 K are observed at the lowest coverages studied. Above 0.020 ML coverage, a high temperature desorption feature appears at 226 K, which is assigned to kink site adsorption. Above 0.077 ML coverage, a low temperature shoulder appears, corresponding to terrace adsorption. Multilayer desorption is seen at higher monolayer coverages and occurs at 157 K and 170 K as seen in the Fig. S6 (ESI†).

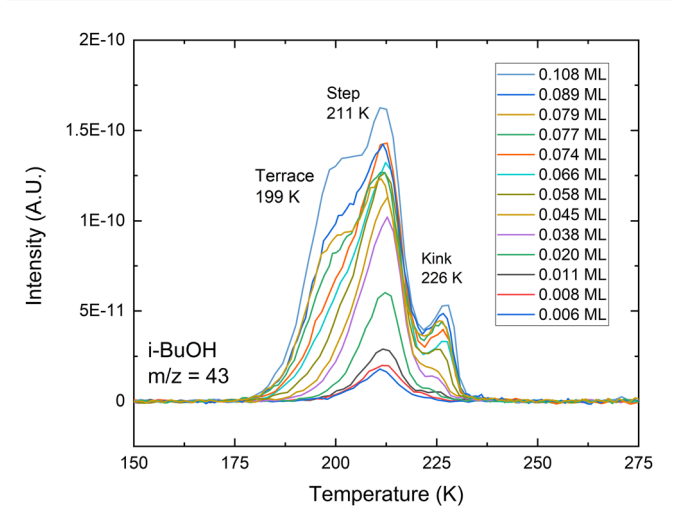


Fig. 5 Sub-monolayer desorption of i-BuOH on Au(111), m/z = 43reported for all experiments, ( $\beta = 0.80 \pm 0.01 \, \text{K s}^{-1}$ ).

#### Redhead analysis prefactor discussion

To better compare desorption features for the small alcohols, a Redhead first order approximation calculation was conducted to convert desorption temperatures into desorption energies. A common issue with using the Redhead equation is choosing an appropriate pre-exponentional factor (prefactor). Prefactors typically increase with molar mass for small adsorbates, and have been found to increase with increasing alkane chain length on MgO(100), C(0001), Pt(111), and PdO(101).34-37 Increases in prefactors are related to the translational and rotational entropy gains upon molecular desorption, which are generally greater for larger molecules. 37,38 Small alcohols C<sub>1</sub>-C<sub>4</sub> on TiO<sub>2</sub>(110) have a desorption prefactor that increases with size from  $\log \nu = 15.4 \text{ s}^{-1}$  to  $\log \nu = 17.5 \text{ s}^{-1}$  on Ti cationic metal sites, and  $\log \nu = 15.0 \text{ s}^{-1}$  to  $\log \nu = 16.5 \text{ s}^{-1}$  on oxygen sites.<sup>37</sup> As Au is much less reactive than TiO<sub>2</sub>, these prefactors are likely overestimates for alcohols adsorbed to Au(111).

Desorption energies were calculated for monolayer desorption sites for all alcohols using the Redhead approximation for first order desorption. This method requires a known preexponential factor ( $\nu$ ) and carries an error of  $\pm 1.5\%$  for values of  $10^{13} \ge \nu/\beta \ge 10^8$ , which all quantitatively reported data falls within.<sup>39</sup> In addition, we estimate the error in our experimental system to be a maximum of  $\pm 5$  K, which is reflected in reported desorption energies as shown in Fig. 6. The desorption energies and error associated with  $\pm 5$  K have been tabulated in Table S1 (ESI†). Also included in Table S1 (ESI†) are the smaller 1.5% error values from the Redhead analysis for comparison. The pre-exponential factor for MeOH desorption from Au(111)

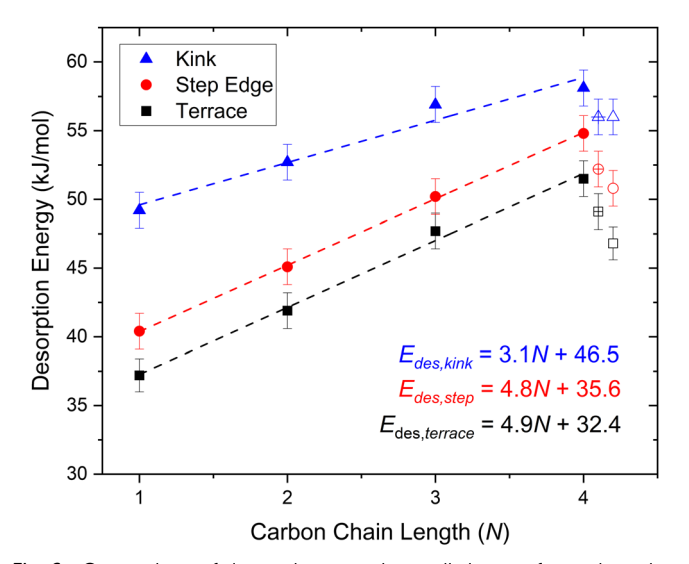


Fig. 6 Comparison of desorption energies at distinct surface adsorption sites with increasing carbon chain length (blue triangles for kinks, red circles for step edges, and black squares for terraces). Primary alcohol i-BuOH data are shown as open plus symbols, offset on the x-axis by 0.1 for clarity. Secondary alcohol 2-BuOH data are shown as open symbols, offset on the x-axis by 0.2 for clarity. Linear best fits for primary alcohol desorption of MeOH, EtOH, 1-PrOH and 1-BuOH from each site are shown. Error bars correspond to experimental errors in desorption temperatures of  $\pm 5$  K.

has previously been calculated via inversion analysis as  $10^{11.3\pm1.1}~{\rm s}^{-1}$  by Gong et al.<sup>5</sup> The pre-exponential factors for the desorption of EtOH, 1-PrOH, and 2-BuOH were not reported in other works, but have been calculated here from known desorption energies, temperatures, and parameters<sup>1,3,4</sup> using the relationship proposed by Redhead<sup>39,40</sup>

$$\nu = \left(\frac{E_{\text{des}}\beta}{RT_{\text{des}}^2\theta_0^{n-1}}\right) e^{E_{\text{des}}/RT_{\text{des}}} \text{ for } n > 0$$
 (1)

where  $E_{\text{des}}$  is the desorption energy,  $T_{\text{des}}$  is the temperature of maximum desorption rate,  $\theta$  is the initial coverage, and n is the order of desorption.

Desorption energy ranges were reported from multilayer to terrace desorption in previous TPD studies for EtOH, 1-PrOH, and 2-BuOH on Au(111).1,3-5 The lower end of reported desorption energy ranges represents multilayer desorption for each alcohol, so prefactor values were calculated from maximum energies reported. The calculated prefactors according to this method are  $\log \nu = 12.3 \text{ s}^{-1}$  for EtOH and 1-PrOH, and  $\log \nu = 12.2 \text{ s}^{-1}$  for 2-BuOH. An application of this method to the case of MeOH returns a value of  $\log \nu = 12.0 \text{ s}^{-1}$ . This value falls within calculated error for the inversion analysis prefactor<sup>5</sup> of MeOH on Au(111) (log  $\nu$  = 11.3  $\pm$  1.1 s<sup>-1</sup>). Thus, we conclude that the prefactor value for the desorption of the small alcohols lies near  $\log \nu = 12.0 \text{ s}^{-1}$ .

The experimentally calculated prefactor for MeOH desorption<sup>5</sup> from Au(111) (10<sup>11.3</sup> s<sup>-1</sup>) is considered highly reliable, as inversion analysis is a well-accepted and rigorous technique. 35,36,40 This experimental value is quite small compared to that of other experimentally studied systems and theoretical values. Thus, the values of pre-exponential factors for the desorption of small alcohols C<sub>1</sub>-C<sub>4</sub> may be 3-5 orders of magnitude smaller than for metal oxide systems or predicted by theoretical calculations. Furthermore, based on the entropic consideration for small alcohol desorption at the temperatures reported, a 1012 prefactor is reasonable according to transition state theory.<sup>38</sup> As such, the desorption energies calculated below use the set of experimentally calculated prefactor of 10<sup>12</sup> for all alcohols studied. Prefactors were determined based on terrace desorption sites, but these same values are also used for defect sites, which will nominally have slightly different prefactors due to differences in binding at these sites. It is assumed that these prefactor differences will be negligible since the entropy gain upon desorption is smaller for small molecules. The errors associated with choosing a prefactor  $(\pm 10^{1})$  are shown in Table S1 (ESI†), but it is important to note that regardless of reasonable prefactors chosen for the calculation of desorption energies, the reported trends and phenomena for small alcohols in Fig. 6 persist.

#### Desorption energy comparison for small alcohols

Fig. 6 shows a plot of the calculated surface site desorption energies for all alcohols studied. Desorption energy generally increases with alcohol size and decreasing coordination number of the adsorption site, and primary alcohol desorption energies

(MeOH, EtOH, 1-PrOH, 1-BuOH) increase linearly with carbon chain length at distinct adsorption sites. A discussion of the molecular packing structure of small alcohols on Au(111) is warranted to distinguish differences in desorption energies. All of the alcohols studied bind atop or near atop on Au(111) through a lone pair of electrons on the oxygen. 10,24,27,41 Lowtemperature STM previously has shown the formation of extended H-bonded networks of MeOH, EtOH, and 1-PrOH on Au(111) where these alcohols maximize H-bonding and vdW between molecules, forming long zigzag chains where the carbon chains point out perpendicularly from the OH bonds. 10,24 As the carbon chain length of primary alcohols increases, both vdW interactions between the carbon chain and Au surface and adjacent carbon chains increase. While the molecular scale selfassembly of 1-BuOH has not yet been studied on Au(111) at low temperatures, the linear trends for primary small alcohols shown in Fig. 6 indicate that 1-BuOH forms long, extended H-bonded chains similar to those observed for MeOH, EtOH, and 1-PrOH, as illustrated in Fig. 7(A).

#### Terrace desorption energies of butanol isomers

In addition to the primary alcohols, the secondary alcohol 2-BuOH was also studied and is shown in Fig. 6 as open symbols, slightly offset from 1-BuOH for clarity. An analysis of desorption energies of 1- and 2-BuOH provides insight towards the nature of adsorbate-adsorbate interactions for these two alcohols. Though these molecules are isomers and bind to the Au(111) surface through the oxygen lone pair, <sup>24</sup> 1-BuOH is stabilized to significantly higher temperatures on the Au(111) surface and follows the linear trend in desorption energy established by the three smallest primary alcohols, as shown in Fig. 6. The effect of lateral interactions on binding strength is evident from the difference in 1- vs. 2-BuOH desorption energies. Previous LT-STM experiments show that 2-BuOH packs in chiral tetramers on Au(111), facilitating

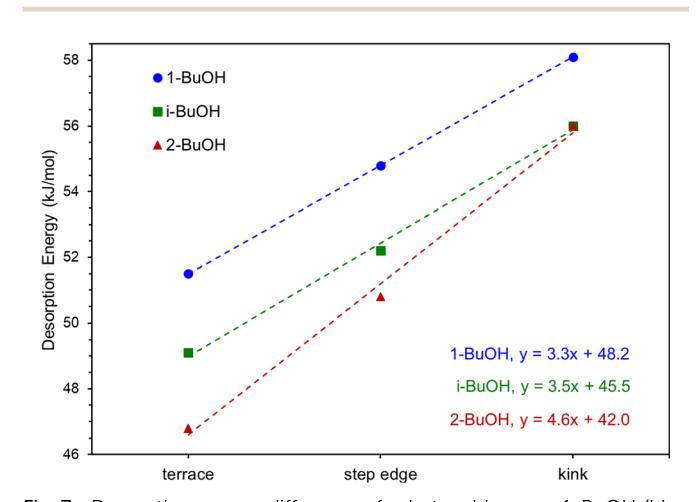
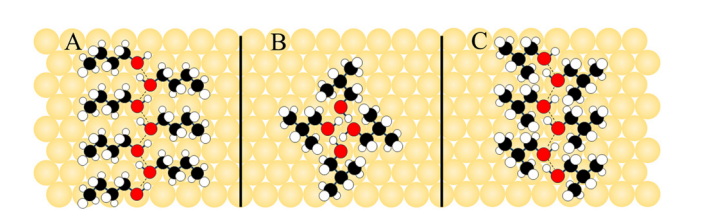


Fig. 7 Desorption energy differences for butanol isomers 1-BuOH (blue circles), i-BuOH (green squares), and 2-BuOH (red triangles) at terrace, step edges, and kink sites. Primary alcohol desorption trends (Fig. 6) and the known packing structure of 2-BuOH allows predictions to be made for the unknown packing structures of 1-BuOH and i-BuOH.

weaker intermolecular interactions compared to the paired zig-zag chains formed by primary alcohols.24 While 1-BuOH adsorbed to terrace sites desorbs with an energy of 51.5  $\pm$ 1.3 kJ mol $^{-1}$ , 2-BuOH desorbs with an energy of 46.8  $\pm$ 1.3 kJ mol<sup>-1</sup> and does not trend with desorption energies of primary alcohols. The desorption energy for 2-BuOH on terraces is in good agreement with previous studies of 2-BuOH on Au(111), where terrace desorption energies for 2-butanol were similar to that of 1- and 2-PrOH. 1,4 The difference in adsorption and desorption character is attributed to the packing behaviour of 1- and 2-BuOH on Au terraces, which dictates the strength of stabilizing intermolecular interactions for molecules adsorbed to the surface. The increased steric hindrance of adsorbed 2-BuOH relative to 1-BuOH results in significantly weaker lateral interactions and lower desorption energies for the secondary alcohol.

The desorption of i-BuOH from Au(111) was also studied and reveals further insight towards the molecular packing of alcohols adsorbed on the Au(111) surface. Fig. 6 shows i-BuOH desorption energies as open plus symbols, offset for clarity. Isobutanol desorbs from Au(111) terrace sites with an energy of  $49.1 \pm 1.3 \text{ kJ mol}^{-1}$ , which falls between the desorption energy values for 1- and 2-BuOH, as shown in Fig. 6 and 7. As with 1-BuOH, the energetics of i-BuOH desorption from the Au(111) terrace inform a more developed understanding of i-BuOH molecular packing on Au(111). The adsorption energy of i-BuOH on Au(111) terraces (49.1 kJ mol<sup>-1</sup>) is less than that of 1-BuOH (51.5 kJ mol<sup>-1</sup>), and greater than that of 2-BuOH (46.8 kJ mol<sup>-1</sup>). Though the desorption of i-BuOH stands energetically between 1- and 2-BuOH, it much more closely aligns with the slope of the 1-BuOH trendline, and thus the trend of primary alcohol desorption energies shown in Fig. 7.

As a primary alcohol, it is possible that the H-bonding structure of i-BuOH more closely resembles that of 1-BuOH than 2-BuOH, though the branched carbon chain of i-BuOH may cause greater repulsion between adsorbed molecules packed on the Au(111) surface. The enhanced repulsion between neighbouring carbon chains is expected to contribute to the slightly lesser desorption energy from the Au(111) terrace of i-BuOH compared to 1-BuOH. Therefore, the desorption energy trends of i-, 1-, and 2-BuOH suggest that i-BuOH forms long extended chains rather than tetramer units. Fig. 8 shows suggested packing models for 1-BuOH (Fig. 8(A)) and i-BuOH as tetramer units (Fig. 8(B)) and extended chains (Fig. 8(C)).



**Fig. 8** Schematics for predicted molecular packing for (A) 1-BuOH extended linear chains, (B) i-BuOH tetramers, and (C) i-BuOH extended linear chains, which are expected to form rather than tetramers based on desorption energies.

While not all possible configurations were considered, the chain and tetramer units are experimentally determined structures for small alcohols. High resolution STM should be conducted to confirm the intermolecular packing structure of i-BuOH in future studies.

#### Small alcohol adsorption on Au(111) defect ites

The desorption energies of primary alcohols at terrace sand step edge sites increases at a rate of  $\sim 4.9 \pm 0.3 \text{ kJ mol}^{-1} \text{ per}$ additional methyl group while kink site desorption energy increases at a rate of 3.1  $\pm$  0.4 kJ mol<sup>-1</sup> per methyl group, as shown in Fig. 6. The difference in the rates is discussed in terms of the molecular-scale packing and interactions on the Au(111) surface. Alcohols adsorbed to terrace sites form extended H-bonded networks, maximizing stabilizing forces related to adsorbate-adsorbate interactions. In contrast, molecules adsorbed to kink sites are more isolated from neighbouring molecules due to the local geometry of the undercoordinated kinks. Therefore, it is predicted that molecules adsorbed to kink sites are more restricted in forming extended H-bonded networks. While the overall desorption energy for alcohols adsorbed to undercoordinated sites is greater, intermolecular interactions (both H-bonding and carbon tail vdW) contribute to the energy much less than a molecule adsorbed to a terrace site. An alternate explanation for the lower rate of increase for kink sites could be related to lateral repulsive interactions at the undercoordinated sites, yet if repulsive interactions were responsible, it would be expected that the desorption energy for molecules adsorbed at kink sites would be lower than that of terrace sites, which is not experimentally observed.

The primary alcohols studied bind to the surface and selfassemble in analogous structures, facilitating the same number of H-bonds. Therefore, changes in desorption with increasing chain length provide evidence towards the diminished role of molecule-surface and intermolecular vdW interactions for alcohols adsorbed at kink sites. Previous DFT studies of a single ethanol molecule adsorbed on Ag(111) indicate that vdW interactions between the ethanol carbon tail and Ag surface are weakened at defect sites.<sup>28</sup> Due to the similarities in the desorption behaviour of alcohols on Ag and Au, it is expected that comparable effects occur at defect sites on Au(111) as well. Interestingly, the rate of increase of desorption energies is the similar for terrace and step edges according to Fig. 6. This indicates that carbon tail vdW forces, while expected to be disrupted at these defects, are not largely affected by step edges. The molecular structure, if aligned along the step edge, could preserve the attractive carbon tail vdW forces as well as the molecule-surface attractive forces.

#### **Butanol comparison on defects**

The comparison of butanol isomer desorption with regard to distinct adsorption sites is necessary for a deeper discussion into the role of surface defects in disrupting self-assembled networks of alcohols on Au(111). A closer analysis of 1-, 2-, and i-BuOH desorption extends this understanding by probing the contributions of H-bonding and carbon tail adsorbate–adsorbate

vdW interactions at distinct adsorption sites. Fig. 7 shows the desorption energies for butanol isomers as a function of adsorption site. The similarity of slopes for 1- and i-BuOH (3.3 kJ mol<sup>-1</sup> and 3.5 kJ mol<sup>-1</sup>) as compared to 2-BuOH (4.6 kJ mol<sup>-1</sup>) is likely due to the predicted packing of long extended chains for 1- and i-BuOH H-bonded structures. Furthermore, the comparison between 1- and 2-BuOH can be used to consider the influence of a smaller H-bonded network (long extended chains vs. tetramers) as well as lessened carbon tail vdW due to a larger distance between molecules in tetramers compared to chains.

While the weak interactions of 1-BuOH adsorbed to Au terrace sites stabilize this alcohol to an energy of 4.7 kJ mol<sup>-1</sup> greater than 2-BuOH, these weak interactions only account for an increase of 4.0 kJ mol<sup>-1</sup> for 1-BuOH adsorbed to step edge sites and 2.1 kJ mol<sup>-1</sup> for 1-BuOH adsorbed to kink sites (compared to 2-BuOH) as shown in Fig. 6 and 7. In addition, for step edges, the difference in desorption energy between 2- and i-BuOH ( $\Delta E_{des} = 1.4 \text{ kJ mol}^{-1}$ ) is smaller than that between 1- and i-BuOH by a factor of  $\sim 2 (\Delta E_{\rm des} = 2.6 \text{ kJ mol}^{-1})$ as shown in Fig. 7. Interestingly, for kink sites, the difference in desorption energies for 1- and i-BuOH and 1- and 2-BuOH is the same ( $\Delta E_{\text{des}} = 2.1 \text{ kJ mol}^{-1}$ ), while there is no difference in desorption energy for 2-BuOH and i-BuOH at kink sites. These differences may be accounted for by molecule-surface vdW interactions because the primary alcohol 1-BuOH is expected to have greater surface interactions than the branched structures of 2- and i-BuOH. Overall, the similarity between 1- and i-BuOH on terraces is related to the intermolecular H-bonded packing, while the similarity between 2- and i-BuOH on step edges and kinks can be attributed to molecular structure interacting with geometrically isolated defect sites. Therefore, the data suggests that both step edge and kink defects inhibit the self-assembly of small alcohol H-bonded molecular networks, as desorption energies of these isomers reflect the distinct nature of their respective networks less with decreasing surface site coordination number.

### Conclusions

TPD experiments highlight subtle differences between adsorbatesurface interactions and weak vdW intermolecular interactions. By investigating the desorption trends of small alcohols on terraces and natural defects sites of Au(111), the effects of molecular packing and undercoordinated defects sites were measured. Desorption trends indicate that 1-BuOH forms H-bonded networks on Au(111) resembling other small primary alcohols, aligning in long extended zigzag chains across the surface that maximize H-bonding and minimize repulsive forces. The desorption trend differences for 1- and 2-BuOH are attributed to differences in the molecular H-bond networks on Au(111) corresponding to zigzag chains and tetramers, respectively. Trends were also used to predict the H-bonded packing structure for i-BuOH, which is expected to form long extended chains. Trends also highlight differences in the rate of increase in desorption energy per methyl group for small,

primary alcohols reliant on their adsorption site. Primary alcohol desorption energies increase by 4.9 kJ mol<sup>-1</sup> per methyl on terrace sites, and only 3.1 kJ mol-1 for kink sites. The smaller energy increase for kink site adsorption is attributed to the disruption of the extended H-bond networks at local geometrically isolated kink sites, which are revealed by butanol isomer studies. The investigation of intermolecular interactions and energetics at undercoordinated defects is important for heterogeneous catalysis where roughened surfaces and nanoparticles are used. Nanostructures with high concentrations of defects will minimize intermolecular interactions while a smooth surface, or larger nanoparticles, maximize these interactions.

### Conflicts of interest

There are no conflicts to declare.

# Acknowledgements

We acknowledge support from the Research Corporation for Science Advancement Cottrell Scholar Award (E. M. M., J. S. B., A. E. B), 4-VA, a collaborative partnership for advancing the Commonwealth of Virginia (L. A. G.), NSF REU CHE-1757874 (H. K.), and the Thomas F. and Kate Miller Jeffress Memorial Trust, Bank of America, Trustee (A. J. G., C. J. R.).

### Notes and references

- 1 T. Yan, J. Gong and C. B. Mullins, J. Am. Chem. Soc., 2009, **131**, 16189–16194.
- 2 D. V. Potapenko, Z. Li, Y. Lou, Y. Guo and R. M. Osgood, J. Catal., 2013, 297, 281-288.
- 3 J. Gong and C. B. Mullins, J. Am. Chem. Soc., 2008, 130, 16458-16459.
- 4 J. Gong, D. W. Flaherty, T. Yan and C. B. Mullins, ChemPhysChem, 2008, 9, 2461-2466.
- 5 J. Gong, D. W. Flaherty, R. A. Ojifinni, J. M. White and C. B. Mullins, J. Phys. Chem. C, 2008, 112, 5501-5509.
- 6 D. T. Boyle, J. A. Wilke, R. M. Palomino, V. H. Lam, D. A. Schlosser, W. J. Andahazy, C. Z. Stopak, D. J. Stacchiola, J. A. Rodriguez and A. E. Baber, J. Phys. Chem. C, 2017, **121**, 7794-7802.
- 7 O. Bondarchuk, Y. K. Kim, J. M. White, J. Kim and B. D. Kay, J. Phys. Chem. C, 2007, 111, 11059-11067.
- 8 S. Biella and M. Rossi, Chem. Commun., 2003, 378-379.
- 9 T. Mallat and A. Baiker, Chem. Rev., 2004, 104, 3037-3058.
- 10 A. E. Baber, T. J. Lawton and E. C. H. Sykes, J. Phys. Chem. C, 2011, 115, 9157-9163.
- 11 Z.-T. Wang, Y. Xu, M. El-Soda, F. R. Lucci, R. J. Madix, C. M. Friend and E. C. H. Sykes, J. Phys. Chem. C, 2017, 121, 12800-12806.
- 12 T. Nilsson Pingel, M. Jørgensen, A. B. Yankovich, H. Grönbeck and E. Olsson, Nat. Commun., 2018, 9, 2722.

13 J. C. F. Rodriguez-Reyes, C. G. F. Siler, W. Liu, A. Tkatchenko, C. M. Friend and R. J. Madix, J. Am. Chem. Soc., 2014, 136, 13333-13340.

- 14 J. Saavedra, H. A. Doan, C. J. Pursell, L. C. Grabow and B. D. Chandler, Science, 2014, 345, 1599-1602.
- 15 C. R. Chang, X. F. Yang, B. Long and J. Li, ACS Catal., 2013, 3, 1693-1699.
- 16 J. Gong, R. A. Ojifinni, T. S. Kim, J. D. Stiehl, S. M. McClure, J. M. White and C. B. Mullins, Top. Catal., 2007, 44,
- 17 K. Sun, M. Kohyama, S. Tanaka and S. Takeda, J. Phys. Chem. C, 2018, 122, 9523-9530.
- 18 R. A. Ojifinni, N. S. Froemming, J. Gong, M. Pan, T. S. Kim, J. M. White, G. Henkelman and C. B. Mullins, J. Am. Chem. Soc., 2008, 130, 6801-6812.
- 19 T. Fujitani, I. Nakamura and M. Haruta, Catal. Lett., 2014, **144**, 1475–1486.
- 20 Z. Liu, E. Huang, I. Orozco, W. Liao, R. M. Palomino, N. Rui, T. Duchoň, S. Nemšák, D. C. Grinter, M. Mahapatra, P. Liu, J. A. Rodriguez and S. D. Senanayake, Science, 2020, 368, 513-517.
- 21 T. J. Lawton, G. Kyriakou, A. E. Baber and E. C. H. Sykes, ChemCatChem, 2013, 5, 2684-2690.
- 22 C. J. Murphy, J. Carrasco, T. J. Lawton, M. L. Liriano, A. E. Baber, E. A. Lewis, A. Michaelides and E. C. H. Sykes, J. Chem. Phys., 2014, 141, 014701.
- 23 T. J. Lawton, J. Carrasco, A. E. Baber, A. Michaelides and E. C. H. Sykes, Phys. Rev. Lett., 2011, 107, 256101.
- 24 M. L. Liriano, A. M. Larson, C. Gattinoni, J. Carrasco, A. E. Baber, E. A. Lewis, C. J. Murphy, T. J. Lawton, M. D. Marcinkowski, A. J. Therrien, A. Michaelides and E. C. H. Sykes, J. Chem. Phys., 2018, 149, 034703.
- 25 W. Foster, K. Miyazawa, T. Fukuma, H. Kusumaatmaja and K. Voïtchovsky, Nanoscale, 2020, 12, 5452-5463.

- 26 K. Voïtchovsky, D. Giofrè, J. José Segura, F. Stellacci and M. Ceriotti, Nat. Commun., 2016, 7, 1-9.
- 27 M. L. Liriano, J. Carrasco, E. A. Lewis, C. J. Murphy, T. J. Lawton, M. D. Marcinkowski, A. J. Therrien, A. Michaelides and E. C. H. Sykes, J. Chem. Phys., 2016, 144, 094703.
- 28 D. A. Schlosser, D. Yehorova, H. Kaleem, E. M. Maxwell, J. S. Baker, M. Z. Gillum, M. C. DePonte, K. Letchworth-Weaver and A. E. Baber, J. Vac. Sci. Technol., A, 2020, 38, 033213.
- 29 W.-L. Yim, T. Nowitzki, M. Necke, H. Schnars, P. Nickut, J. Biener, M. M. Biener, V. Zielasek, K. Al-Shamery, T. Klüner and M. Bäumer, J. Phys. Chem. C, 2007, 111, 445-451.
- 30 D. P. Engelhart, R. J. V. Wagner, A. Meling, A. M. Wodtke and T. Schäfer, Surf. Sci., 2016, 650, 11-16.
- 31 A. E. Baber, T. J. Lawton and E. C. H. Sykes, J. Phys. Chem. C, 2011, 115, 9157-9163.
- 32 X. Liu, B. Xu, J. Haubrich, R. J. Madix and C. M. Friend, J. Am. Chem. Soc., 2009, 131, 5757-5759.
- 33 A. J. Brush, M. Pan and C. B. Mullins, J. Phys. Chem. C, 2012, **116**, 20982–20989.
- 34 S. L. Tait, Z. Dohnálek, C. T. Campbell and B. D. Kay, J. Chem. Phys., 2005, 122, 164707.
- 35 S. L. Tait, Z. Dohnálek, C. T. Campbell and B. D. Kay, J. Chem. Phys., 2005, 122, 164708.
- 36 S. L. Tait, Z. Dohnálek, C. T. Campbell and B. D. Kay, J. Chem. Phys., 2006, 125, 234308.
- 37 C. T. Campbell and J. R. V. Sellers, Chem. Rev., 2013, 113, 4106-4135.
- 38 C. T. Campbell and J. R. V. Sellers, J. Am. Chem. Soc., 2012, **134**, 18109–18115.
- 39 P. A. Redhead, Vacuum, 1962, 12, 203-211.
- 40 A. M. de Jong and J. W. Niemantsverdriet, Surf. Sci., 1990, 233, 355-365.
- 41 W. K. Chen, S. H. Liu, M. J. Cao, Q. G. Yan and C. H. Lu, J. Mol. Struct., 2006, 770, 87-91.